Holocene long- and short-term climate changes off Adélie Land, East Antarctica

Xavier Crosta, Maxime Debret, D. Denis, M. A. Courty, O. Ther

Geochemistry Geophysics Geosystems G3
AN ELECTRONIC JOURNAL OF THE EARTH SCIENCES
Published by AGU and the Geochemical Society

Article
Volume 8, Number 11
30 November 2007
Q11009, doi:10.1029/2007GC001718
ISSN: 1525-2027

Holocene long- and short-term climate changes off Adélie Land, East Antarctica

X. Crosta
UMR-CNRS 5805 EPOC, Avenue des Facultés, F-33405 Talence, France (x.crosta@epoc.u-bordeaux1.fr)

M. Debret
Laboratoire de Glaciologie et de Geophysique de l'Environnement, BP 96, F-38402 St Martin d'Heres, France

D. Denis
UMR-CNRS 5805 EPOC, Avenue des Facultés, F-33405 Talence, France

M. A. Courty
UMR 5198, CNRS-IPH, F-66720 Tautavel, France

O. Ther
UMR-CNRS 5805 EPOC, Avenue des Facultés, F-33405 Talence, France

[1] Diatom data from a marine sediment core give insight on Holocene changes in sea-surface conditions and climate at high southern latitudes off Adélie Land, East Antarctica. The early to mid-Holocene was warmer than the late Holocene with a transition at ~4000 calendar years B. P. Sea ice was less present and spring-summer growing season was greater during the warm period relative to the cold one, thus limiting sea ice diatom production and favoring more open ocean diatom to develop. The long-term Holocene climatic evolution in East Antarctica is explained by a combination of a delayed response to local seasonal insolation changes coupled to the long memory of the Southern Ocean. Abrupt variations of the diatom relative abundances, indicating rapid climate changes, are superimposed to the Holocene long-term trends. Spectral analyses calculate robust frequencies at ~1600 a (where "a" is years), ~1250 a, ~1050 a, ~570 a, ~310 a, ~230 a, ~150–125 a, ~110 a, ~90 a, and ~66 a. Such periods are very close to solar activity cyclicities, except for the periods at ~310 a and ~1250 a, which are close to internal climate variability cyclicities. Wavelet analyses estimate the same periods but indicate nonstationary cyclicities. Rapid climate changes at high southern latitudes may therefore be explained by a combination of external (solar) and internal (thermohaline circulation) forcings.

Components: 9422 words, 8 figures.

Keywords: Antarctica; sea ice; Holocene; insolation; thermohaline circulation.

Index Terms: 9310 Geographic Location: Antarctica (4207); 4901 Paleoceanography: Abrupt/rapid climate change (1605); 4936 Paleoceanography: Interglacial.

Received 12 June 2007; **Revised** 10 October 2007; **Accepted** 23 October 2007; **Published** 30 November 2007.

Crosta, X., M. Debret, D. Denis, M. A. Courty, and O. Ther (2007), Holocene long- and short-term climate changes off Adélie Land, East Antarctica, *Geochem. Geophys. Geosyst.*, *8*, Q11009, doi:10.1029/2007GC001718.

1. Introduction

[2] Marine records [*Leventer et al.*, 1996; *Hodell et al.*, 2001; *Taylor et al.*, 2001; *Brachfeld et al.*, 2002; *Presti et al.*, 2003; *Cunningham et al.*, 1999; *Nielsen et al.*, 2004] and glacial records [*Masson et al.*, 2000; *Masson-Delmotte et al.*, 2004] indicate a warmer early to mid-Holocene and a colder late Holocene. The transition between the warmer Hypsithermal and the colder Neoglacial is found to be more or less abrupt depending on the study area and the proxy used. However, no consensus has been reached about forcing factors of Holocene long-term climate trends at high southern latitudes. The long-term climate evolution at southern latitudes was explained as a response to the decreasing summer insolation at high northern latitudes [*Nielsen et al.*, 2004] or to the decreasing annual mean meridional insolation gradient in the Southern Hemisphere [*Masson et al.*, 2000]. Both mechanisms impact heat transport via their influence on the thermohaline circulation to or from the Southern Ocean. More recently, a modeling experiment demonstrated that long-term climate trends in the Southern Ocean more likely result from a delayed response to local orbital forcing with temperatures lagging seasonal insolation by a few months and winter storage of oceanic warmth below the shallow summer mixed layer [*Renssen et al.*, 2005].

[3] Similarly, marine and glacial records indicate Holocene rapid climate changes at decadal-to-millennial timescales. Little is known about the forcing mechanisms of rapid climate changes in the Southern Ocean because of the lack of high-resolution records, especially in the marine environment. Millennial cycles were related to regional climate change over Antarctica [*Masson et al.*, 2000] involving the strength and extent of the polar vortex [*Delmonte et al.*, 2005]. Similar cycles were found in the South Atlantic possibly indicating a link between Antarctic climate and lower latitudes [*Nielsen et al.*, 2004]. Centennial climate changes of 200–300 a (where "a" is years) [*Leventer et al.*, 1996] and 200 a [*Delmonte et al.*, 2005] were noted to possibly result from solar activity. There is however not enough overlap between the recorded periods and solar activity cyclicities to define a casual relationship. Additionally, internal climate variability involving rapid shifts of the Southern Ocean thermohaline circulation, with periods of 320–360 a and 1060–1100 a, and known as the "Southern ocean flip-flop oscillator" [*Pierce et al.*, 1995; *Drijfhout et al.*, 1996; *Osborn*, 1997] exists.

[4] We present here a high-resolution diatom record from core MD03-2601 retrieved on the Antarctic Continental Shelf off Adélie Land and covering the 9000–1000 years B. P. period. One diatom species group, *Fragilariopsis curta*, is intimately linked to sea ice presence [*Armand et al.*, 2005] while the other species, *Fragilariopsis kerguelensis*, thrives in the open ocean and is rare when sea ice is present during the growing season [*Crosta et al.*, 2005a]. These diatom species therefore were used as proxies to document surface temperatures and sea ice conditions, with a 10 to 20 a resolution in core MD03-2601. Sea ice is one of the fastest reacting, most seasonal geophysical parameter on Earth's surface. Its seasonal cycle is strongly dependent on water temperature, surface air temperatures and wind activity [*Ackley*, 1980] and to incoming solar energy [*Comiso*, 2003; *Haas*, 2003]. It is therefore sensible to investigate past sea ice dynamics to better understand the driving mechanisms of Holocene climate change at high southern latitudes.

2. Material and Methods

2.1. Material

[5] Piston core MD03-2601 was retrieved during MD130 - Images X cruise (CADO – Coring Adélie Diatom Oozes) in February 2003 on board R.V. Marion Dufresne II with the logistic support of the French IPEV (Institut Paul Emile Victor). Core MD03-2601 was retrieved at 66°03.07′S, 138°33.43′E in 746 m water depth in one of the small depressions composing the D'Urville Trough (Figure 1). The Trough incises the shelf out to the shelf break and is bounded to the east by the Adélie Bank and to the west by the Dibble Bank. The trough has an average depth of 600–700 m and consists of a series of small depressions reaching a maximum depth of 900–1000 m [*De Santis et al.*, 2003]. These depressions act as funnels, which focus the phytoplankton cells (mainly diatoms [*Wright and van den Enden*, 2000]) produced in the area, thereby increasing their preservation efficiency. Core MD03-2601 is composed of diatom ooze alternating between structureless greenish ooze and green-to-dark green laminations of millimeter to centimeter thickness.

2.2. Stratigraphy

[6] Nine radiocarbon dates were performed on the green material humic fraction of bulk organic matter at the Leibniz Laboratory, Kiel, Germany. Raw ^{14}C dates were calibrated to calendar ages

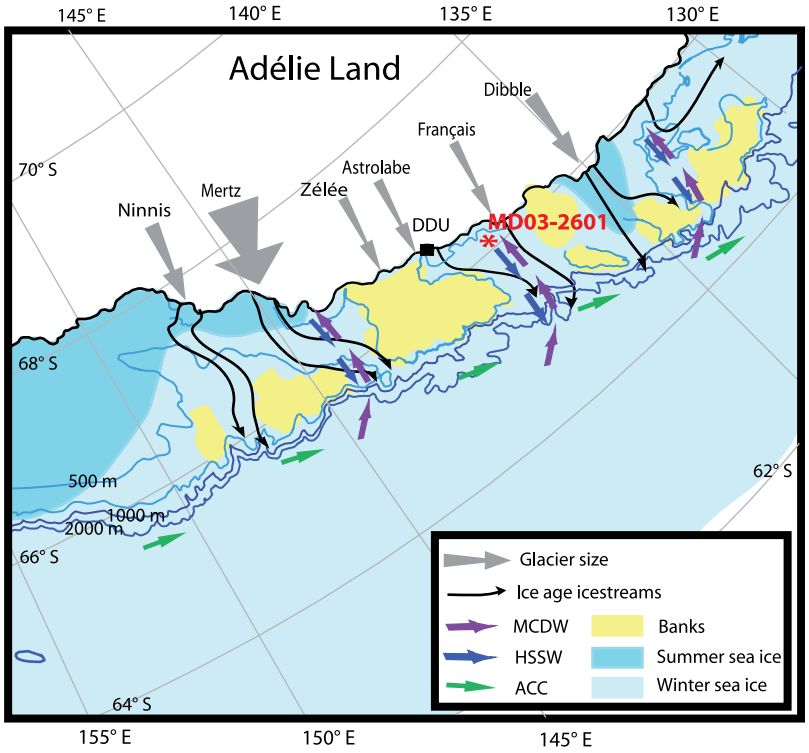

Figure 1. Map showing the location of core MD03-2601 and the bathymetry and the oceanography of the Adélie Land region.

using Bard's polynome [*Bard et al.*, 1998] after applying a 1300 a reservoir age effect [*Ingólfsson et al.*, 1998]. Calibration using another polynome [*Stuiver et al.*, 1998a] provides very similar calendar ages with associated errors of ±100 a at 1σ. Radiocarbon concentration in the Southern Ocean is dominated by the upwelling of Circumpolar Deep Waters at the Antarctic Divergence, which induces an older average reservoir age than the global ocean mean. Circum-Antarctic studies of living mollusks showed that the average correction for reservoir age is 1100–1400 ^{14}C a [*Stuiver et al.*, 1981; *Björck et al.*, 1991; *Gordon and Harkness*, 1992; *Berkman and Forman*, 1996]. The correction for marine reservoir age at high southern latitudes is generally 1300 ^{14}C a [*Ingólfsson et al.*, 1998] except in semi-closed bay systems where the correction can be as high as 2600 ^{14}C a [*Adamson and Pickard*, 1986; *Taylor and McMinn*, 2001] due to input of depleted ^{14}C CO_2 from melting ice and presence of perennial sea ice. Given the location of core MD03-2601 and the oceanography of the area, there is no reason to use a marine reservoir age older than 1300 a.

[7] In core MD03-2601, two samples at 998 cm and 1498 cm yield older dates than expected from the distribution pattern of the other dates (Figure 2). The resulting higher sedimentation rate between these depths is spurious because of congruent low values of the focusing factor and low numbers of laminations [*Denis et al.*, 2007]. Rather than an increase in the sedimentation rate these two dates indicate a greater input of old carbon, possibly in relation to the 4000 years B. P. meteoritic impact [*Courty et al.*, 2007]. A linear regression (r^2 = 0.98) was therefore applied to the nine radiocarbon dates to minimize biases due to old carbon input. The seven other dates closely follow the regression line (Figure 2).

[8] Additional support for using a correction of 1300 a and applying a regression line to the nine dates is provided by the indication of the 4000 years B. P., or 4470 calendar years B. P., meteoritic impact at 1440–1400 cm in core MD03-2601. Exogene material typical of the 4000 years B. P. impact is abundant between 1440 cm and 1400 cm and subsequently diluted by hemipelagic material up-core until 1000 cm [*Courty et al.*, 2007]. This external control point falls in line with the regres-

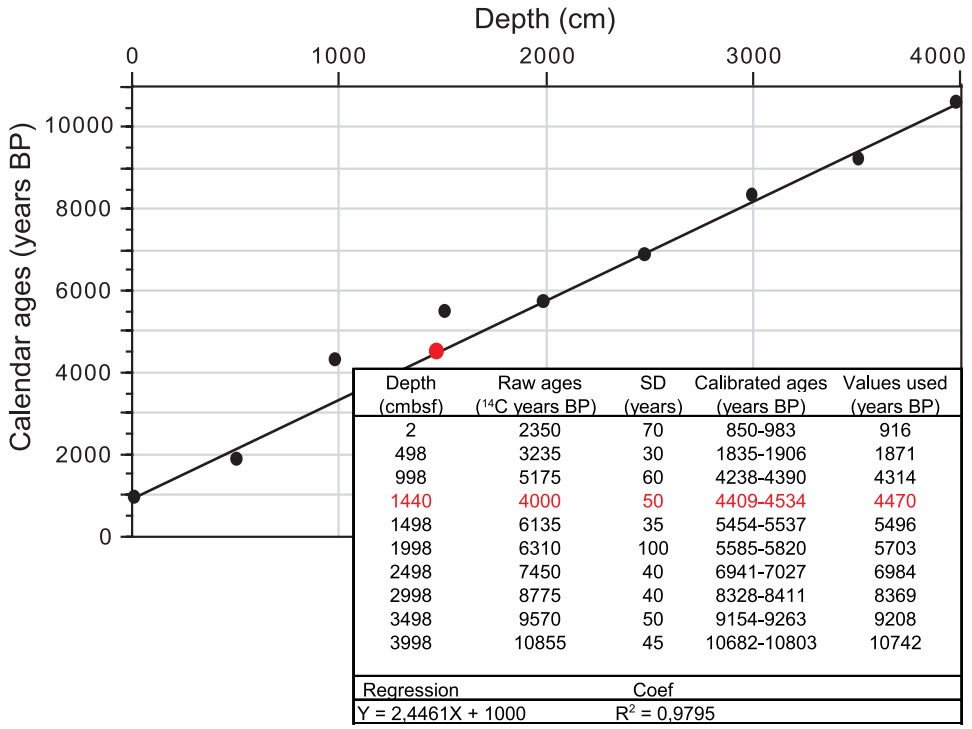

Depth (cmbsf)	Raw ages (^{14}C years BP)	SD (years)	Calibrated ages (years BP)	Values used (years BP)
2	2350	70	850-983	916
498	3235	30	1835-1906	1871
998	5175	60	4238-4390	4314
1440	4000	50	4409-4534	4470
1498	6135	35	5454-5537	5496
1998	6310	100	5585-5820	5703
2498	7450	40	6941-7027	6984
2998	8775	40	8328-8411	8369
3498	9570	50	9154-9263	9208
3998	10855	45	10682-10803	10742

Regression	Coef
Y = 2,4461X + 1000	R^2 = 0,9795

Figure 2. Calibrated radiocarbon ages versus depth in core MD03-2601. Radiocarbon ages were calibrated using Bard's polynome [*Bard et al.*, 1998] and assume a constant reservoir age of 1300 a [*Ingólfsson et al.*, 1998]. Black dots represent radiocarbon dates performed on humic acids. The red dot represents the depth at which the 4000 yr B. P. meteoritic impact was evidenced [*Courty et al.*, 2007].

sion line (Figure 2, red dot), thus supporting the ^{14}C-based stratigraphy.

[9] The core covers the 9000–1000 calendar years B. P. (cal yr B. P.) period with an average sedimentation rate of 0.4 cm.a^{-1} (Figure 2), in agreement with early investigations of East Antarctica sediments [*Domack*, 1988].

2.3. Diatom Analysis

[10] Diatom identification was performed every 4 to 8 cm providing a 10–20 a resolution. Samples were prepared and analyzed according to the technique described by *Rathburn et al.* [1997]. Diatom counts followed *Schrader and Gersonde* [1978] and *Laws* [1983]. Around 350 diatom valves were counted in each sample at a magnification of 1250. Diatoms were identified to species or species group level, and the relative abundance of each was determined as the fraction of diatom species against total diatom abundance in the sample. More details about slide preparation, diatom identification and statistical treatment are described by *Crosta et al.* [2004].

2.4. Spectral Analysis

[11] Two software programs of spectral analysis, Wavelet [*Torrence and Compo*, 1998] and Redfit 3.8 [*Schulz and Muldesee*, 2002], were used to decipher information from the diatom records in the frequency domain. Wavelet analyses were performed on the whole time series (9000–1000 years B. P.) whereas Redfit was applied separately on the Hypsithermal (9000–3900 years B. P.) and Neoglacial (3900–1000 years B. P.) periods as the Fourier transform is disturbed by the sharp jump in diatom relative abundances at the Hypsithermal-Neoglacial transition.

[12] The climatic system is typical example of nonstationary processes, in which frequency content and statistical properties change through time. Wavelet analysis (WA) presents the advantage of describing nonstationarities, i.e., discontinuities, changes in frequency or magnitude [*Torrence and Compo*, 1998]. Redundancy of the continuous wavelet transform is used to produce a time/frequency or time/scale mapping of power distribution, called the local wavelet spectrum (or scalogram). As a major advantage with respect to

classical Fourier analysis, the local wavelet spectrum allows direct visualization of the changing statistical properties in stochastic processes with time. A wave number of 10 was used, this choice offering a good trade-off between frequency and temporal resolution for the time series analyzed herein. To avoid edge effects and spectral leakage that are produced by the finite length of the time series, all series were zero-padded to twice the data length. However, zero-padding causes the lowest frequencies near the edges of the spectrum to be underestimated as more zeros enter the series. The area delineating this region is known as the cone of influence and marks those parts of the spectrum where energy bands are likely to be less powerful than they actually are because edge effects are becoming important.

[13] Redfit 3.8 is based on a Lomb-Scargle Fourier transform combined with a Welch-Overlapped-Segment-Averaging procedure for consistent spectral estimates [*Schulz and Muldesee*, 2002]. Redfit has two advantages. First, it works with unevenly spaced time series which avoid tapering of high frequencies. Second, it estimates the red-noise spectrum which allows the identification of significant frequencies. Spectral analysis was performed with 1000 Monte-Carlo simulations, an oversampling factor of 4 for the Fourier transform, four segments with a 50% overlapping, and a Welch window-type. Red-noise spectrum of 90% was selected to highlight significant frequencies.

3. Results and Discussion

3.1. Reconstruction of Antarctic Paleoclimate Using Diatoms

[14] Antarctic sea ice diatom populations are largely represented by *Fragilariopsis* species with *Fragilariopsis curta* and *F. cylindrus* (the *F. curta* group hereafter) as the dominant taxa. Sediment traps experiments have shown that relative abundances of the *F. curta* group in the phytoplankton increase southward with increasing sea ice cover and decreasing temperature [*Gersonde and Zielinski*, 2000]. Similarly, investigation of surface water samples between New Zealand and the Ross Sea demonstrated increasing abundances of the *F. curta* group during spring with increasing sea ice concentration [*Burckle et al.*, 1987]. *Fragilariopsis curta* develops at the retreating sea ice edge in relatively stable and nutrient-rich environments. The surface water seasonal production results in a southward positive gradient of the *F. curta* group in surface sediment at the basin scale [*Zielinski and Gersonde*, 1997; *Armand et al.*, 2005] and at the local scale [*Leventer*, 1992]. Investigation of the sediment micro-structure in core MD03-2601 confirmed the spring occurrence of the *F. curta* group and its greater occurrence during the colder Neoglacial period that during the warmer Hypsithermal period during which cryophilic *Fragilariopsis* are mainly represented by *F. rhombica* [*Denis et al.*, 2006]. It is therefore believed that higher relative abundances of the *F. curta* group in sediments indicate reduced growing season due to denser sea ice cover and late waning. Relative abundances of the *F. curta* group have been successfully used to reconstruct presence of sea ice during the late Pleistocene through qualitative [*Gersonde and Zielinski*, 2000] or transfer function [*Crosta et al.*, 2004] approaches.

[15] The Southern Ocean plankton is dominated by *F. kerguelensis* which achieves its highest abundances during summer just south of the Polar Front [*Kozlova*, 1962, 1966; *Froneman et al.*, 1995]. Low occurrences of this diatom have been observed along the Antarctic Coast [*Gersonde*, 1984; *Fenner et al.*, 1976] consistent with a growing season that is too short to allow *F. kerguelensis* to bloom. The resulting surface sediment distribution of *F. kerguelensis* reflects its production in surface waters with highest abundances south of the Polar Front and decreasing abundances both northward and southward [*Crosta et al.*, 2005a; *Cortese and Gersonde*, 2007]. Investigation of the sediment micro-structure in core MD03-2601 demonstrated the summer occurrence of *F. kerguelensis* and the greater occurrence during the warmer Hypsithermal period that during the colder Neoglacial period [*Denis et al.*, 2006]. It is believed that a longer growing season during the Hypsithermal, a function of the early retreat and late waxing of sea ice promoted *F. kerguelensis* to become more abundant.

3.2. Diatom Records

[16] The records of the *F. curta* group and *F. kerguelensis* are strongly anti-correlated giving a correlation coefficient of 0.6 and present a strong amplitude shift in relative abundances at the Hypsithermal-Neoglacial transition (Figures 3a and 3b). The anti-correlation results from the opposite ecological preferences of the two taxa. The jump results from the loss or gain of competitivity of one species in response to changing environmental conditions, especially in sea surface temperature

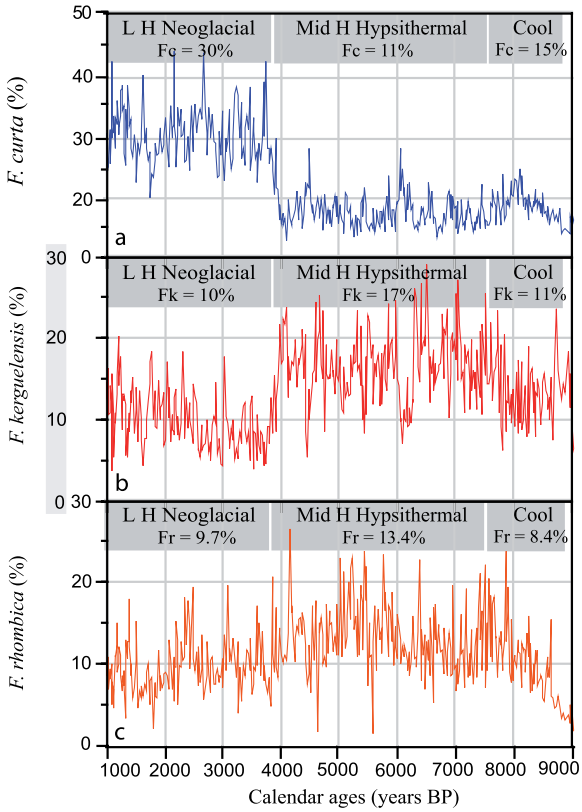

Figure 3. Relative abundances of (a) the *Fragilariopsis curta* group and (b) *F. kerguelensis* and (c) *F. rhombica* versus calendar ages in core MD03-2601. Mean abundances of the three species are reported for each climatic period. Fc, *F. curta*; Fk, *F. kerguelensis*; Fr, *F. rhombica*; LH, late Holocene; Mid H, mid Holocene.

and sea ice cover. The diatom records must be approached on two scales: the Holocene long-term scale and the decadal-to-millennial scale.

3.2.1. Holocene Long-Term Trends

[17] At the long-term scale, the Holocene can be separated in three distinct periods. Between 8700 cal yr B. P. and 7700 cal yr B. P., both the *F. curta* group and *F. kerguelensis* present relative abundances around 10–15% (Figures 3a and 3b). Between 7700 cal yr B. P. and 3900 cal yr B. P., the *F. curta* group shows abundances around 10% while *F. kerguelensis* shows abundances around 15–20%. Between 3900 cal yr B. P. and 1000 cal yr B. P., the *F. curta* group represents 25–35% of the total diatom assemblage while *F. kerguelensis* represents 5–15% of the assemblage. These patterns indicate cooler conditions during the 8700–7700 cal yr B. P. period, warmer conditions during the 7700–3900 yr B. P. period and colder conditions during the 3900–1000 cal yr B. P. period. The transition between the Hypsithermal and the Neoglacial periods appears very abrupt in the diatom records (Figures 3a and 3b). This jump may be related to a threshold in the diatom ecological response to a small climate change. Today, the surface water temperature is around 0.5°C and sea ice covers the region around 9 months per year. These conditions represent the upper ecological limit for *F. curta* and the lower ecological limit for *F. kerguelensis*. Indeed, *F. curta* relative abundances in 228 modern surface sediments from the Southern Ocean are maximum between 0°C and 0.5°C and decrease abruptly above 1°C [*Armand et al.*, 2005]. *Fragilariopsis kerguelensis* relative abundances in modern sediments are conversely highest between 1°C and 6°C and decrease sharply below 1°C [*Crosta et al.*, 2005a]. A small sea-surface temperature change across the 1°C boundary, and associated sea ice conditions, will therefore completely change the diatom species dominating the siliceous assemblage. Evaluating relative abundances of *F. curta* and *F. kerguelensis* during the Hypsithermal and Neoglacial periods based on their distribution in modern surface sediments [*Armand et al.*, 2005; *Crosta et al.*, 2005a] allows us to estimate a ~1°C cooling and ~1 month increase in sea ice cover at the Hypsithermal-Neoglacial transition. This is confirmed by model output which estimates that spring temperatures were ~1.5°C warmer during the Hypsithermal than the Neoglacial [*Renssen et al.*, 2005]. Warmer spring temperatures are unfavorable to *F. curta* that become less competitive relative to *F. rhombica* in such conditions [*Armand et al.*, 2005]. The faster sea ice melting increased the length of the summer season [*Denis et al.*, 2006], thus allowing *F. kerguelensis* to build up greater biomass. The situation is reversed for the Neoglacial period with colder spring temperatures and shorter summer season favorable to *F. curta* production relative to *F. rhombica* and *F. kerguelensis* (Figure 3).

[18] The diatom records confirm the climatic interpretations based on the $\delta^{13}C_{org}$ record in core MD03-2601 [*Crosta et al.*, 2005b]. They are also in agreement with climatic interpretations based on temperature anomalies recorded at EPICA Dome C [*Masson-Delmotte et al.*, 2004], on sea-surface temperatures reconstructed for the Southern Atlantic [*Nielsen et al.*, 2004] and on magnetic susceptibility changes from the Antarctic Peninsula [*Brachfeld et al.*, 2002], all records showing a similar cool event during the early Holocene, a warm mid-Holocene and a cold late Holocene.

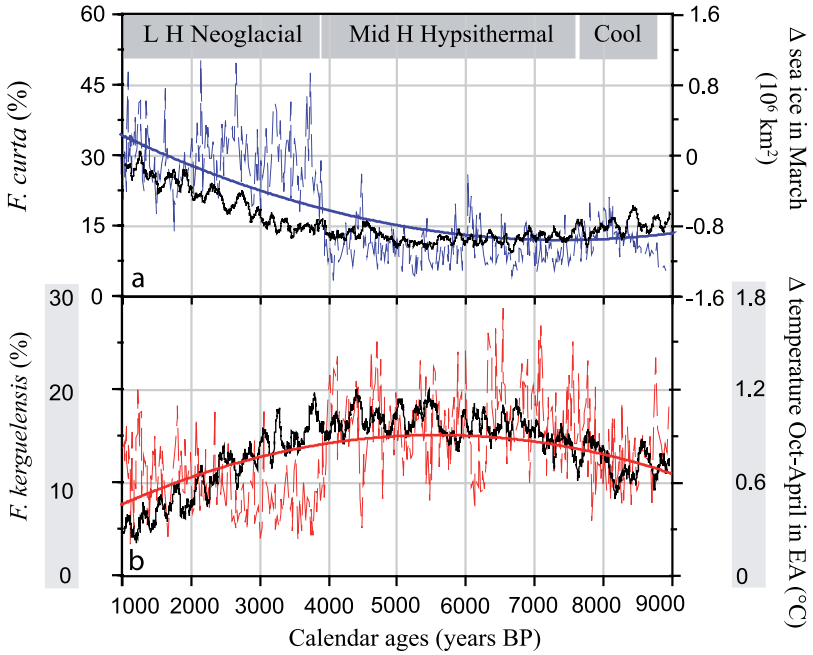

Figure 4. Relative abundances of (a) the *Fragilariopsis curta* group (blue dotted line) and (b) the *Fragilariopsis kerguelensis* (red dotted line) versus calendar ages in core MD03-2601. Polynomial regressions indicate the Holocene first-order evolution for the *F. curta* group (Figure 4a, blue solid line) and the *F. kerguelensis* (Figure 4b, red solid line) and are compared to simulated time series of the March sea ice area (Figure 4a, black line) and the October-to-April temperature for East Antarctica over the last 9000 a (Figure 4b, black line), plotted as deviation from the preindustrial mean [*Renssen et al.*, 2005].

Timing of the climatic periods is however not in phase in the different regions, which may reflect intrinsic discrepancies in core stratigraphies, core resolutions and proxies, or different climate regional evolution. A recent model experiment relates the earlier Holocene warming in West Antarctica to a stronger sea ice reduction in the western sector of the Southern Ocean than in the eastern sector [*Renssen et al.*, 2005]. The 9000-yr transient experiment also estimates a mid-Holocene warm phase surrounded by cooler early and late Holocene periods.

[19] The summer sea ice area quantified by the model [*Renssen et al.*, 2005], presented as a difference from the preindustrial mean, is compared to relative abundances of the *F. curta* group over the last 9000 cal years. Summer sea ice cover was lower than today during the 7500–4000 cal yr B. P. period when it started increasing to reach its preindustrial values ~1000 a ago (Figure 4a, black line). The sharp jump in *F. curta* relative abundances at 3900 yr B. P. precludes a direct comparison with summer sea ice area. We therefore applied a polynomial regression to extract the first order long-term trend in *F. curta* abundances (Figure 4a, blue solid line). The long-term evolution of the *F. curta* group is very similar to summer sea ice area with lower diatom occurrence during the Hypsithermal (7700–3900 cal yr B. P.) when summer sea ice is less present and with greater diatom abundances during the Neoglacial (3900–1000 cal yr B. P.) when summer sea ice is more extended.

[20] The reconstructed surface temperatures for the spring-summer season [*Renssen et al.*, 2005] are compared to *F. kerguelensis* relative abundances over the last 9000 cal yr B. P. Surface temperatures were ~1°C warmer during the 7500–3800 cal yr B. P. period they started decreasing to reach their preindustrial values ~1000 a ago (Figure 4b, black line). The long-term trend of *F. kerguelensis* abundances (Figure 4b, red solid line) presents a similar evolution than the spring-summer temperature trend with higher occurrence during the Hypsithermal (7700–3900 cal yr B. P.) when temperatures are warmer and lower abundances during the Neoglacial (3900–1000 cal yr B. P.) when temperatures are cooler.

[21] The Holocene long-term trends in sea ice area and surface temperatures are explained by a combination of a delayed response to local orbital forcing with temperatures lagging seasonal insola-

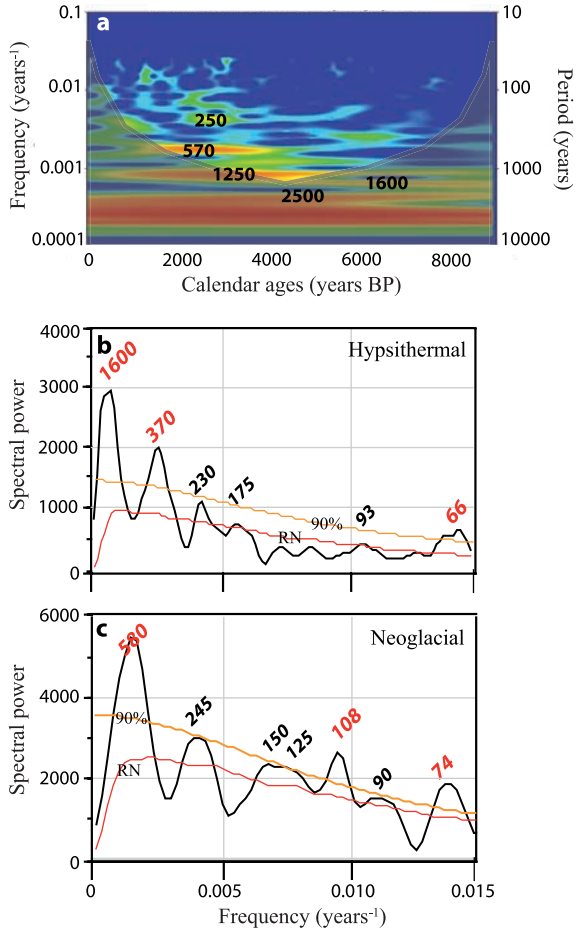

Figure 5. Spectral analyses of the *F. curta* gp relative abundances. (a) Wavelet analysis for the whole Holocene, (b) Redfit analysis for the Hypsithermal period, and (c) Redfit analysis for the Neoglacial period. Significant cycles (red values) are identified as peaks crossing the red noise (RN) and 90% confidence level lines.

tion by few months and winter storage of oceanic warmth below the shallow summer mixed layer until the next winter thus producing year-round warm conditions at high southern latitudes [*Renssen et al.*, 2005]. Sea ice is not a simple passive parameter responding to climate changes. At each step, sea ice acts as a strong amplifying factor through albedo and insulation feedbacks.

[22] Holocene long-term changes were previously explained through connections to summer insolation at high northern latitudes [*Nielsen et al.*, 2004], through the annual mean meridional insolation gradient in the Southern Hemisphere [*Masson et al.*, 2000] or through the seasonal difference in insolation [*Lamy et al.*, 2002]. The diatom records in core MD03-2601 support a more direct driver of Holocene long-term climate evolution at high southern latitudes in which local insolation modulated by local feedbacks is the central process.

3.2.2. Short-Term Changes

[23] The two diatom records show high amplitude variations at several shorter timescales. Amplitudes are up to 15% for centennial timescales and up to 10% for decadal timescales in both records (Figure 3). Variability of each species is greater when the contribution of that species is higher. Spectral and wavelet analyses were therefore performed (1) to determine periodicities of diatom relative abundance variations, (2) to determine whether the cyclicities are persistent throughout the Holocene, and (3) to determine what forcings may trigger the observed rapid changes.

3.2.2.1. Spectral Analyses of the Diatom Records

[24] Wavelet analyses were performed on the total data set while Redfit analyses were performed on the Neoglacial and Hypsithermal periods. For the Hypsithermal, wavelet analysis of the *F. curta* group estimates only one significant period centered at ~1600 a (Figure 5a). The same period is also evidenced by Redfit along with a set of shorter periods. Significant periods at the 90% confidence level appear at ~370 a and ~66 a while additional periods above the red noise appear at ~230 a, ~175 a and ~93 a (Figure 5b). For the Neoglacial, wavelet analysis calculates periods at ~1250 a, ~570 a and ~250 a (Figure 5a). The ~1250 a cyclicity is not estimated by Redfit because of its nonstationary state. Conversely, Redfit identifies periods at ~580 a, ~108 a and ~74 a at the 90% confidence level and periods at ~245 a, 150–125 a and ~90 a above the red noise (Figure 5c).

[25] For the Hypsithermal, wavelet analysis of *F. kerguelensis* relative abundances calculates ~1600 a, ~1050 a, ~570 a and ~320 a (Figure 6a). Redfit also identifies cyclicities at ~1600 a and ~575 a accompanied by several shorter periods at ~310 a and ~110 a significant at the 90% confidence level and additional periods at ~240 a, ~160 a and ~86 a above the red noise (Figure 6b). For the Neoglacial, wavelet analysis estimates periods at ~580 a and ~280 a (Figure 6a). Redfit similarly identifies the period at ~270 a along with shorter cyclicities at ~170 a and ~110 a (Figure 6c). All periods are significant at the 90% confidence level.

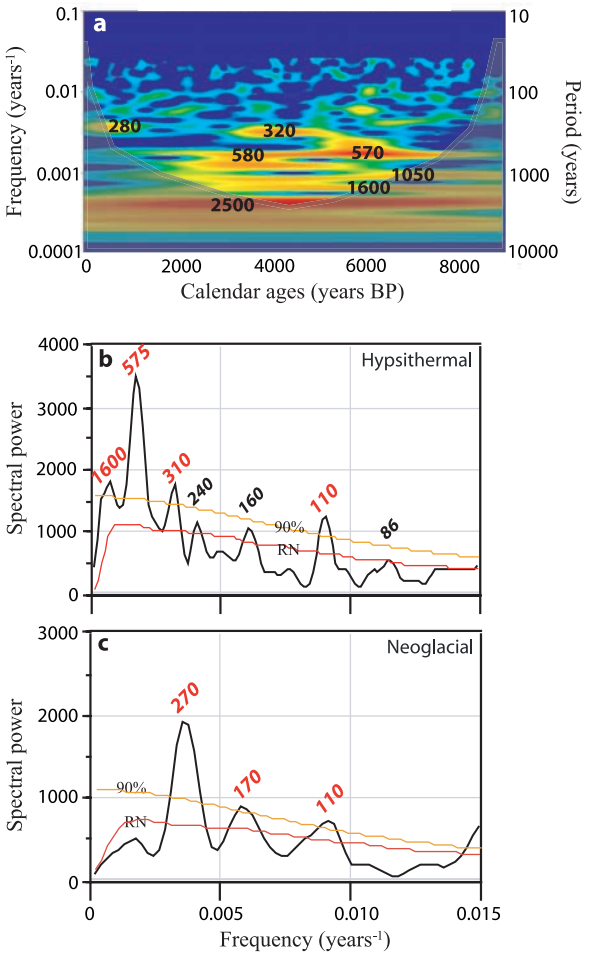

Figure 6. Spectral analyses of *F. kerguelensis* relative abundances. (a) Wavelet analysis for the whole Holocene, (b) Redfit analysis for the Hypsithermal period, and (c) Redfit analysis for the Neoglacial period. Significant cycles (red values) are identified as peaks crossing the red noise (RN) and 90% confidence level lines.

[26] During the Hypsithermal, changes *F. kerguelensis* abundance are up to 15–20% while changes in *F. curta* occurrence is only 5–10%. The situation is reversed for the Neoglacial period with variations of greater amplitude for the *F. curta* group than for *F. kerguelensis*. Cyclicities calculated on *F. kerguelensis* relative abundances during the Hypsithermal and periods estimated on occurrence of the *F. curta* group during the Neoglacial therefore appear more robust. Very consistent cyclicities at ~580 a, ~240 a, ~150 a, ~110 a, ~90 a and ~75 a are thence calculated for both climatic periods. Cyclicities at ~1600 a, ~1050 a and ~310 a are only present during the Hypsithermal while a period at ~1250 a is only present during the Neoglacial.

3.2.2.2. Coherency With Solar Activity Cycles

[27] Local cyclic climate changes, as recorded by the diatom assemblages in core MD03-2601, are very similar to known periods of solar activity. A maximum entropy method applied to a Holocene tree ring $\Delta^{14}C$ record from North America shows periodicities of 805 a, 385 a, 232 a, 208 a, 131 a, 105 a and 88 a [*Damon and Sonnett*, 1991]. Similarly, a multitapered method applied to the ^{14}C production rate recorded in Irish bog trees yields periodicities of 860 a, 500 a, 358 a, 291 a, 228 a, and 209 a [*Turney et al.*, 2005].

[28] For confirmation of solar activity periodicities and for harmonization with our own results, we applied both wavelets and Redfit to the $\Delta^{14}C_{residual}$ record [*Stuiver et al.*, 1998b]. Spectral analyses were performed on the whole Holocene record as not abrupt step exists in the radiocarbon record. Wavelet analysis identifies periods of ~1600 a, ~950 a and ~550 a during the Hypsithermal and a period of ~550 a during the Neoglacial (Figure 7a). Redfit calculates periods at ~930 a, ~540 a, ~350 a, ~230–205 a, ~150–125 a, ~105 a, ~88 a and ~68 a (Figure 7b). Such cyclicities are very close to the periods identified from the composite diatom record, except for the period at ~1250 a restricted to the Neoglacial.

[29] Within the accuracy of our radiocarbon chronology, our results thus indicate cyclic climate changes at decadal-to-centennial scales in coincidence with known solar cycles. This similarity suggests that a link may be likely between solar activity and the ultimate geophysical parameter influencing diatom production at high southern latitudes, namely sea ice cover and seasonal cycle.

[30] A few studies from Antarctica [*Masson et al.*, 2000; *Delmonte et al.*, 2005] and the Southern Ocean [*Domack et al.*, 1993; *Leventer et al.*, 1996; *Domack and Mayewski*, 1999; *Nielsen et al.*, 2004] have inferred a solar forcing of local climate during the Holocene, and they were generally restricted to pluri-centennial periodicities because of the lack of high accumulation sites. However, two studies indicate pluri-decadal cyclicities. Spectral analysis of diatom-based sea-surface temperatures in the Polar Front Zone of the South Atlantic identified periods of 1220 a, 1070 a, 400 a and 150 a [*Nielsen et al.*, 2004]. Spectral analysis of the variability in clay and medium-silt content over the last 9000 years B. P. in one core from the Antarctic Peninsula

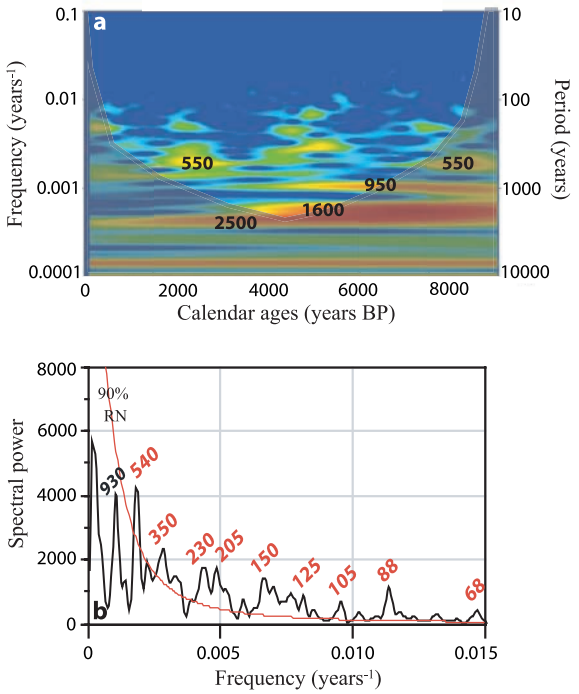

Figure 7. Spectral analyses of the $\Delta^{14}C_{residual}$ [*Stuiver et al.*, 1998b]. (a) Wavelet analysis and (b) Redfit analysis for the whole Holocene. Significant cycles (red values) are identified as peaks crossing the red noise (RN) and 90% confidence level lines.

however demonstrated cycles at 400 a, 200 a, 100 a and 70 a and were related to solar or multidecadal forcing [*Warner and Domack*, 2002]. The presence of high-resolution records outside the Southern Ocean confirm our own results and provide a more global view of rapid cyclic climate change. A long-term Tasmanian tree ring record of warm season temperatures presents significant periods of 77–80 a and 200 a [*Cook et al.*, 1996] possibly attributed to solar activity. Many studies from the Northern Hemisphere [*Poore et al.*, 2003; *Mayewski et al.*, 2004] and particularly from the northern high latitudes [*Campbell et al.*, 1998; *Sarnthein et al.*, 2003; *Hu et al.*, 2003] highlight the Sun-Earth relations at decadal-to-centennial timescales. Therefore a solar forcing of rapid climate changes at high latitudes during the Holocene is plausible, although the Sun-Earth relation is not always well expressed depending on the reconstructed parameter and the location of the cores.

3.2.2.3. Possible Amplifying Mechanisms of Solar Activity

[31] Energy changes associated with solar activity are small amounting 0.1% (0.34 W.m^{-2}) during the 11 a cycle [*Friis-Christensen*, 2000], 0.2% to 0.6% (0.7 W.m^{-2} to 2 W.m^{-2}) on secular cycles [*Lean and Rind*, 1998; *Mendoza*, 1997], and 1.3% (4 W.m^{-2}) on the Holocene timescale [*Renssen et al.*, 2006]. The question to address is how the climate system reacts to changes in solar forcing. Amplifying feedbacks are necessary to explain the amplitude of the climate response. Two possible mechanisms have been postulated, both of them working through atmospheric processes. They may work alone or in concert, and are superposed to other climate forcing and internal climate variability [*Rind*, 2002] to introduce additional climate variability at decadal to centennial timescales around the average climate conditions prevailing during the Neoglacial and the Hypsithermal.

[32] The first feedback mechanism involves UV radiations and ozone production. Solar spectral irradiance fluctuations are proportionally larger at short wavelengths and UV radiation carries ~20% of the total solar energy variability [*Lean*, 1991]. During solar maxima, more UV radiation is absorbed by the stratospheric ozone hence raising the temperature and producing stronger winds in the lower stratosphere that subsequently penetrate in the troposphere where they lead to a relocation of storm tracks and pressure cells [*Shindell et al.*, 1999] (Figure 8). More recurrent storms and poleward distribution of low pressure cells may enhance the mechanical break-up of the sea ice [*Enomoto and Ohmura*, 1990; *Simmonds*, 1996]. Strong variations in the number of storms reaching the Adélie Land have been observed at the pluriannual timescale during the Holocene [*Denis et al.*, 2006]. Additionally, penetration of the stratospheric warm temperature anomaly of few tenths of a degree Kelvin into the lower troposphere [*Shindell et al.*, 1999] may reduce sea ice freezing. Both processes therefore alter the sea ice seasonal cycle and the biosiliceous production toward less cryophilic and more open ocean diatoms. Conversely, solar minima induce less storms, equatorward displacement of the low-pressure cells and injection of a cool temperature anomaly into the lower troposphere leading to later sea ice break-up and earlier freezing. A shorter growth season implies more cryophilic and less open ocean diatoms.

[33] The second feedback involves the cosmic ray flux and cloud cover. The net forcing of the global cloud cover has been estimated at 17–35 W.m^{-2} cooling due to greater occurrence of low clouds (cooling) than high clouds (warming), which makes global cloud cover a very effective ampli-

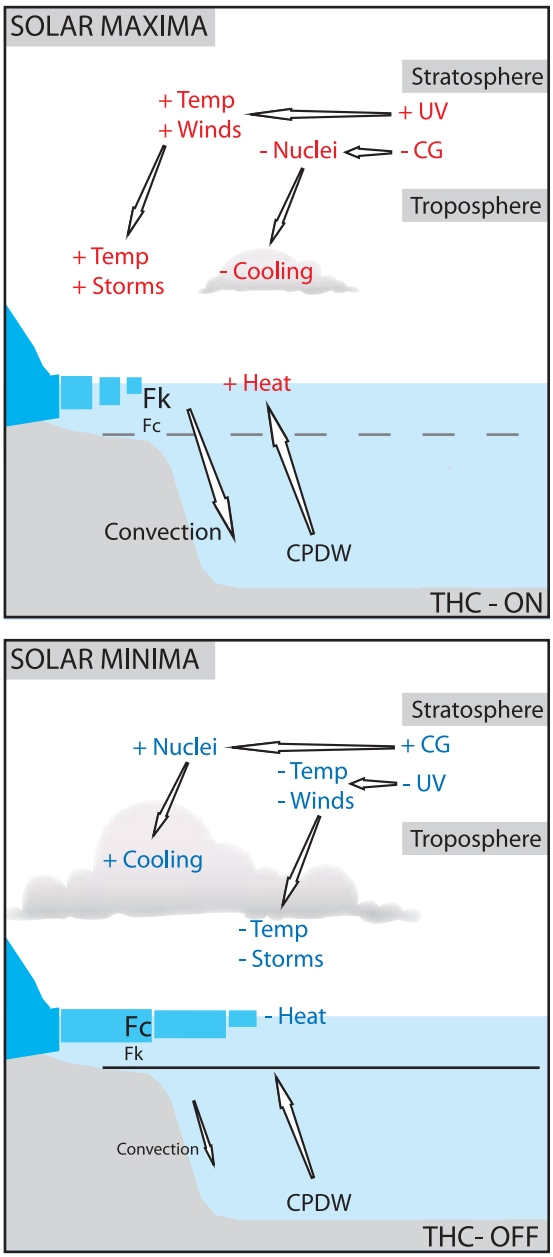

Figure 8. Conceptual model of processes affecting sea ice extent, and subsequently diatom production, during (top) solar maxima and THC-ON states and (bottom) solar minima and THC-OFF states. Fc, *F. curta*; Fk, *F. kerguelensis*; CG, cosmic grains; CPDW, Circumpolar Deep Water; THC, thermohaline circulation.

fying mechanism for climate forcing [*Svensmark*, 2000]. The relationship between the intensity of the galactic cosmic rays and low cloud cover is still under debate, mainly about the handling of the observational data [*Damon and Laut*, 2004]. Some authors found that global cloud cover appears highly correlated with cosmic ray flux and anti-correlated with solar activity [*Svensmark and Friis-Christensen*, 1997]. Other authors state that such relationship does not exist but prone that both cosmic rays and low cloud cover are tied to solar activity, thence showing a certain degree of correlation even if cosmic rays do not play any role in cloud formation [*Laut*, 2003]. It is believed that less cosmic particles reach the atmosphere during events of high solar activity, which decreases the amount of nuclei for cloud condensation thus reducing the cloud cover [*Marsh and Svensmark*, 2000] (Figure 8). Less cooling of the lower atmosphere is therefore expected during high solar irradiance anomaly. Conversely, more low clouds are expected during low solar activity thus providing additional cooling of the lower atmosphere. It is possible that temperature changes in the lower atmosphere due to cloud cover strongly affect sea ice formation in autumn and decay in spring when environmental conditions are chaotic and sea ice cover unconsolidated. Strong connection between the flux of cosmic rays and Earth's climate has been evidenced for at the millennial timescale over the last 200,000 a [*Sharma*, 2002; *Christl et al.*, 2004].

3.2.2.4. Coherency With Internal Climate Variability

[34] Antarctic surface temperature and sea ice fields present cyclic variations at several periods. The Antarctic Circumpolar Wave [*White and Peterson*, 1996], the Antarctic Dipole [*Yuan*, 2004] and the Antarctic Oscillation [*Silvestri and Vera*, 2003] are mainly atmospheric manifestations with periods of 3–4 a. Longer cyclicities nest in the slow-reacting ocean that undergoes self-sustained oscillations with timescales of 320–360 a and 1060–1100 a [*Pierce et al.*, 1995].

[35] Spectral analyses of the diatom records evidence periods at 310–370 and 1050 a during the Hypsithermal (Figures 5b and 6b) and 1250 a during the Neoglacial (Figure 5c). Such periods are very close to the above mentioned internal climate cyclicities. The two shorter cycles are also expressed in the $\Delta^{14}C_{residual}$ record. It is therefore possible that both external and internal forcing work together to amplify centennial-scale changes in surface temperature and sea ice cover as evidenced for the Northern Hemisphere [*Renssen et al.*, 2006]. Conversely, the period at ~1250 a is not expressed in solar activity and it may result from internal climate variability alone.

[36] Similar cycles of 200–300 a were noted in down-core records of diatom abundances from the

Antarctic Peninsula and were related to solar activity [*Leventer et al.*, 1996]. Periods of high primary productivity are driven by the presence of a stabilized water column induced by weaker winds, thermal warming and sea ice melting. It is however possible that variation in diatom production are driven by cyclic changes in injection of warmer-than-local circumpolar water, thus promoting sea ice melting and surface water stratification.

[37] Indeed, the self-sustained oscillations involve strong variations in the Southern Ocean thermohaline circulation and the Antarctic Circumpolar Current strength [*Drijfhout et al.*, 1996; *Osborn*, 1997]. The "Southern Ocean flip-flop oscillator" purports movement between two steady states: one characterized by strong stratification, expanded sea ice cover and reduced convection, and the other characterized by weak stratification, reduced sea ice cover, strong convection and active thermohaline circulation. The 320–360 a and the 1060–1100 a cycles are coupled with the latter one being an amplification of the former period. The movement from one state to the other is related to the time necessary to reduce stratification in the Southern Ocean and to eventually reverse the density gradient, i.e., when deep waters become lighter than surface waters. When the Antarctic Ocean is stratified, the heat brought by the Circumpolar Deep Water accumulates in subsurface, which slowly decreases the vertical gradient until surface waters become denser than subsurface ones. Reduction of the density gradient is accompanied by greater vertical diffusion of heat that melts the sea ice cover [*Pierce et al.*, 1995] (Figure 8). Convection thence strongly increases and is compensated by the input of fresher and warmer water from the north that eventually sinks along with newly formed Antarctic Bottom Water and is advected eastward by the stronger Antarctic Circumpolar Current and ultimately in the global conveyor belt [*Drijfhout et al.*, 1996]. Diffusion of the accumulated heat to the atmosphere slowly cools subsurface waters, which increases again the density gradient and stabilizes the water column. Less heat is thus available to melt sea ice that expands again. The Antarctic Circumpolar Current weakens and the convection slows down reducing the thermohaline circulation and the propagation of the density anomaly.

[38] The bottom line of the above mentioned model experiments [*Pierce et al.*, 1995; *Drijfhout et al.*, 1996; *Osborn*, 1997] is that self-sustained oscillations induce cyclic variations in input of warmer water and in resulting sea ice extent that are central to diatom production. During the Thermohaline-On state, convection brings warmer deep waters up which reduces sea ice cover [*Pierce et al.*, 1995]. This situation is detrimental to *F. curta* production but favorable for *F. rhombica* and F. *kerguelensis* development. The situation is reversed during the Thermohaline-Off state when the strong stratification promotes sea ice expansion and slower sea ice melting because of negligible input of warmer waters from below and from the north [*Pierce et al.*, 1995]. This situation is favorable to *F. curta* production at the expense of *F. rhombica* and *F. kerguelensis*.

4. Conclusion

[39] Diatom data from one core retrieved in the Adélie Trough, East Antarctica, document sea ice cover and sea surface temperature changes during the Holocene with a 10–20 a resolution. Diatoms, in agreement with model output, indicate that the mid-Holocene was ~1–2°C warmer than the late Holocene. Sea ice was present for 3–4 weeks less per year off Adélie Land during the Hypsithermal (7700–3900 cal yr B. P.) than the Neoglacial (3900–1000 cal yr B. P.). Its seasonal distribution was also certainly different. The Holocene long-term trends in sea ice area and surface temperatures are explained by a combination of a delayed response to local orbital forcing and the long memory of the Southern Ocean. The diatom data additionally show high amplitude variations at several shorter timescales. Spectral analyses estimate very consistent cyclicities at ~580 a, ~240 a, ~150 a, ~110 a, ~90 a and ~75 a for both climatic periods; cyclicities at ~1600 a, ~1050 a and ~310 a present only during the Hypsithermal; and a period at ~1250 a present only during the Neoglacial. Such cyclicities are very close to know periods of solar activity and internal climate variability, both forcing certainly acting together at congruent frequencies. It is however necessary to obtain similar high-resolution marine records from other Antarctic coastal areas to better assess the impact of solar and internal forcings. More specifically, because sea ice responds so quickly it is expected that its long-term evolution may be out-of-phase in East and West Antarctica but that short-term changes may be concomitant. Given the importance of Antarctic sea ice on the global climate, it is also essential to model sea ice seasonal cycles more precisely taking into account natural and anthropogenic forcing to better under-

stand whether its recent retreat [*Curran et al.*, 2003] is part of a natural cycle or deeply affected by human activity. The present study may serve as a basis to decipher the recent warming from the natural cyclicities, and thus to better constrain climatic and paleoclimatic models.

Acknowledgments

[40] We thank Hans Renssen, Raimund Muscheler, Michel Crucifix, Pieter Grootes, and Jean-Robert Petit for data and discussions. We are grateful to Nicolas Massei for assistance with the wavelets analyses. Extended thanks go to Amy Leventer and an anonymous reviewer for helpful comments that improved the manuscript. We personally thank people from the Images X (CADO) cruise and from the NSF-funded NBP0101 cruise for data and suggestions concerning the D'Urville Trough. Logistical support was provided by IPEV-TAAF. Financial support for this study was provided by the project TARDHOL through the national EVE-LEFE program (INSU-CNRS). This is EPOC contribution 1679.

References

Ackley, S. F. (1980), A review of sea-ice weather relationships in the Southern Hemisphere, in *Proceeding of the Canberra Symposium: Sea Level, Ice, and Climatic Change*, edited by I. Allision, *IAHS Publ.*, *131*, 127–159.

Adamson, D., and J. Pickard (1986), Cenozoic history of the Vestfold Hills, in *Antarctic Oasis: Terrestrial Environments and History of the Vestfold Hills*, edited by J. Pickard, pp. 63–98, Academic, Sydney, Australia.

Armand, L., X. Crosta, O. Romero, and J. J. Pichon (2005), The biogeography of major diatom taxa in Southern Ocean sediments. 1. Sea ice related species, *Palaeogeogr. Palaeoclimatol. Palaeoecol.*, *223*, 93–126.

Bard, E., M. Arnold, B. Hamelin, N. Tisnerat-Laborde, and G. Cabioch (1998), Radiocarbon calibration by means of mass spectrometric Th-230/U-234 and C-14 ages of corals: An updated database including samples from Barbados, Mururoa and Tahiti, *Radiocarbon*, *40*(3), 1085–1092.

Berkman, P. A., and S. L. Forman (1996), Pre-bomb radiocarbon and the reservoir correction for calcareous marine species in the Southern Ocean, *Geophys. Res. Lett.*, *23*, 363–366.

Björck, S., C. Hjort, O. Ingólfsson, and G. Skog (1991), Radiocarbon dates from the Antarctic Peninsula region—Problems and potential, *Quat. Proc.*, *1*, 55–65.

Brachfeld, S. A., S. K. Banerjee, Y. Guyodo, and G. D. Acton (2002), A 13200 year history of century to millennial-scale paleoenvironmental change magnetically recorded in the Palmer Deep, western Antarctic Peninsula, *Earth Planet. Sc. Lett.*, *194*, 311–326.

Burckle, L. H., S. S. Jacob, and R. B. McLaughlin (1987), Late austral spring diatom distribution between New Zealand and the Ross Ice Shelf, Antarctica: Hydrography and sediment correlations, *Micropaleontology*, *33*(1), 74–81.

Campbell, I. D., C. Campbell, M. J. Apps, N. W. Rutter, and A. B. G. Bush (1998), Late Holocene—1500 yr climatic periodicities and their implications, *Geology*, *26*(5), 471–473.

Christl, M., A. Mangini, S. Holzkämper, and C. Spötl (2004), Evidence for a link between the flux of galactic cosmic rays and Earth's climate during the past 200,000 years, *J. Atmos. Sol. Terr. Phys.*, *66*, 313–322.

Comiso, J. C. (2003), Large-scale characteristics and variability of the global sea ice cover, in *Sea Ice: An Introduction to Its Physics, Chemistry, Biology and Geology*, edited by D. N. Thomas and G. S. Dieckmann, pp. 112–142, Blackwell, Oxford, U. K.

Cook, E., B. M. Buckley, and R. D. D'Arrigo (1996), Interdecadal climate oscillations in the Tasmanian sector of the Southern Hemisphere: Evidence from tree rings over the past three millennia, in *Forcing Mechanisms of the Last 2000 Years*, *NATO ASI Ser.*, *Ser. I*, vol. 141, edited by P. D. Jones, R. S. Bradley, and J. Jouzel, pp. 141–160, Springer, New York.

Cortese, G., and R. Gersonde (2007), Morphometric variability in the diatom Fragilariopsis kerguelensis: Implications for Southern Ocean paleoceanography, *Earth Planet. Sci. Lett.*, *257*, 526–544.

Courty, M. A., et al. (2007), Impact fingerprints of the 4 kyr BP dust event based on archaeological, soil, lake and marine archives, paper presented at General Assembly of the European Geosciences Union, Vienna, 16 –20 April .

Crosta, X., A. Sturm, L. Armand, and J. J. Pichon (2004), Late Quaternary sea ice history in the Indian sector of the Southern Ocean as recorded by diatom assemblages, *Mar. Micropaleontol.*, *50*, 209–223.

Crosta, X., O. Romero, L. Armand, and J. J. Pichon (2005a), The biogeography of major diatom taxa in Southern Ocean sediments. 2. Open Ocean related species, *Palaeogeogr. Palaeoclimatol. Palaeoecol.*, *223*, 66–92.

Crosta, X., J. Crespin, I. Billy, and O. Ther (2005b), Major factors controlling Holocene $\delta^{13}C_{org}$ changes in a seasonal sea-ice environment, Adélie Land, East Antarctica, *Global Biogeochem. Cycles*, *19*, GB4029, doi:10.1029/2004GB002426.

Cunningham, W., A. Leventer, J. T. Andrews, A. E. Jennings, and K. J. Licht (1999), Late Pleistocene-Holocene marine conditions in the Ross Sea, Antarctica: Evidence from the diatom record, *Holocene*, *9*(2), 129–139.

Curran, M. A. J., T. D. van Ommen, V. L. Morgan, K. L. Phillips, and A. S. Palmer (2003), Ice core evidence for Antarctic sea ice decline since the 1950's, *Science*, *302*, 1203–1206.

Damon, E., and P. Laut (2004), Pattern of strange errors plagues solar activity and terrestrial climate data, *Eos Trans. AGU*, *39*, 370–374.

Damon, E., and C. P. Sonnett (1991), Solar and terrestrial components of the atmospheric ^{14}C variation spectrum, in *The Sun in Time*, edited by C. P. Sonnett, M. S. Giampapa, and M. S. Matthews, pp. 360–388, Univ. of Ariz. Press, Tucson.

De Santis, L., G. Brancolini, and F. Donda (2003), Seismostratigraphic analysis of the Wilkes Land continental margin (East Antarctica): Influence of glacially driven processes on the Cenozoic deposition, *Deep Sea Res., Part II*, *50*, 1563–1594.

Delmonte, B., J. R. Petit, G. Krinner, V. Maggi, J. Jouzel, and R. Udisti (2005), Ice core evidence for secular variability and 200-year dipolar oscillations in atmospheric circulation over East Antarctica, *Clim. Dyn.*, *24*, 641–654.

Denis, D., X. Crosta, S. Zaragosi, O. Romero, B. Martin, and V. Mas (2006), Seasonal and sub-seasonal climate changes recorded in laminated diatom ooze sediments, Adélie Land, East Antarctica, *Holocene*, *16*(8), 1137–1147.

Denis, D., X. Crosta, S. Schmidt, D. Carson, R. Ganeshram, N. van Ash, J. Crespin, O. Ther, and I. Billy (2007), Climate and productivity changes off Adélie Land (East Antarctica) during the Holocene: Decadal to millennial timescales, paper presented at Ninth International Conference on Paleoceanography, Joint Oceanogr. Inst., Shanghai, China, 2–7 Sept.

Domack, E. W. (1988), Biogenic facies in the Antarctic glacimarine environment: Basis for a polar glacimarine summary, *Palaeogeogr. Palaeoclimatol. Palaeoecol.*, *63*, 357–372.

Domack, E. W., and P. Mayewski (1999), Bi-polar ocean linkages: Evidence from Late-Holocene Antarctic marine and Greenland ice-core records, *Holocene*, *9*, 247–251.

Domack, E. W., T. A. Mashiotta, L. A. Burkley, and S. E. Ishman (1993), 300-year cyclicity in organic matter preservation in Antarctic fjord sediments, in *The Antarctic Paleoenvironment: A Perspective on Global Change, Part Two*, *Antarct. Res. Ser.*, vol. 60, edited by J. P. Kennett, and D. A. Warnke, pp. 265–272, AGU, Washington, D. C.

Drijfhout, S., C. Heinze, M. Latif, and E. Maeir-Reimer (1996), Mean circulation and internal variability in an ocean primitive equation model, *J. Phys. Oceanogr.*, *26*, 559–580.

Enomoto, H., and A. Ohmura (1990), The influences of atmospheric half-yearly cycle on the sea ice extent in the Antarctic, *J. Geophys. Res.*, *95*(C6), 9497–9511.

Fenner, J., H. J. Schrader, and H. Wienigk (1976), Diatom phytoplankton studies in the southern Pacific Ocean, composition and correlation to the Antarctic Convergence and its paleoecological significance, *Initial Rep. Deep Sea Drill. Proj.*, *35*, 757–813.

Friis-Christensen, (2000), Solar variability and climate: A summary, *Space Sci. Rev.*, *94*, 411–421.

Froneman, P. W., R. Perissinotto, C. D. McQuaid, and R. K. Laubscher (1995), Summer distribution of net phytoplancton in the Atlantic sector of the Southern Ocean, *Pol. Biol.*, *15*, 77–84.

Gersonde, R. (1984), Siliceous microorganisms in sea ice and their record in sediments in the southern Weddell Sea (Antarctica), in *Proceedings of the Eighth Diatom Symposium, Paris*, pp. 549–566, Koeltz, Koenigstein, Germany.

Gersonde, R., and U. Zielinski (2000), The reconstruction of late Quaternary Antarctic sea-ice distribution—The use of diatoms as a proxy for sea-ice, *Palaeogeogr. Palaeoclimatol. Palaeoecol.*, *162*, 263–286.

Gordon, J. E., and D. D. Harkness (1992), Magnitude and geographic variations of the radiocarbon content in Antarctic marine life: Implications for reservoir corrections in radiocarbon dating, *Quat. Sci. Rev.*, *11*, 697–708.

Haas, C. (2003), Dynamics versus thermodynamics: The sea ice thickness distribution, in *Sea Ice: An Introduction to its Physics, Chemistry, Biology and Geology*, edited by D. N. Thomas, and G. S. Dieckmann, pp. 333–372, Blackwell Sci., Oxford, U. K.

Hodell, D. A., S. L. Kanfoush, A. Shemesh, X. Crosta, C. D. Charles, and T. P. Guilderson (2001), Abrupt cooling of Antarctic surface waters and sea ice expansion in the South Atlantic sector of the Southern Ocean at 5000 cal yr BP, *Quat. Res.*, *56*, 191–198.

Hu, F. S., D. Kaufman, S. Yoneji, D. Nelson, A. Shemesh, Y. Huang, J. Tian, G. Bond, B. Clegg, and T. Brown (2003), Cyclic variation and solar forcing of Holocene climate in the Alaskan Subarctic, *Science*, *301*, 1890–1893.

Ingólfsson, O., et al. (1998), Antarctic glacial history since the Last Glacial Maximum: An overview of the record on land, *Antarct. Sci.*, *10*(3), 326–344.

Kozlova, O. G. (1962), Specific composition of diatoms in the waters of the Indian sector of the Antarctic, *Trudy Inst. Okeonol. Akad. Nauk SSSR*, *61*, 3–18.

Kozlova, O. G. (1966), *Diatoms of the Indian and Pacific Sectors of the Antarctic*, 185 pp., Isr. Program for Sci. Transl., Natl. Sci. Found., Washington, D. C.

Lamy, F., C. Rühlemann, D. Hebbeln, and G. Wefer (2002), High- and low-latitude climate control on the position of the southern Peru-Chile Current during the Holocene, *Paleoceanography*, *17*(2), 1028, doi:10.1029/2001PA000727.

Laut, P. (2003), Solar activity and terrestrial climate: An analysis of some purported correlations, *J. Atmos. Sol. Terr. Phys.*, *65*, 801–812.

Laws, R. A. (1983), Preparing strewn slides for quantitative microscopical analysis: A test using calibrated microspheres, *Micropaleontology*, *24*, 60–65.

Lean, J. (1991), Variations in the Sun's radiative output, *Rev. Geophys.*, *29*, 505–535.

Lean, J., and D. Rind (1998), Climate forcing by changing solar radiation, *J. Clim.*, *11*, 3069–3094.

Leventer, A. (1992), Modern distribution of diatoms in sediments from the Georges V coast, Antarctica, *Mar. Micropaleontol.*, *19*, 315–332.

Leventer, A., E. W. Domack, S. E. Ishman, S. Brachfeld, C. E. McClennen, and P. Manley (1996), Productivity cycles of 200–300 years in the Antarctic Peninsula region: Understanding linkages among the sun, atmosphere, oceans, sea ice, and biota, *Geol. Soc. Am. Bull.*, *108*(12), 1626–1644.

Marsh, N. D., and H. Svensmark (2000), Low cloud properties influenced by cosmic rays, *Phys. Rev. Lett.*, *85*, 5004–5007.

Masson, V., et al. (2000), Holocene climate variability in Antarctica based on 11 ice-core isotopic records, *Quat. Res.*, *54*, 348–358.

Masson-Delmotte, V., B. Stenni, and J. Jouzel (2004), Common millennial-scale variability of Antarctic and Southern Ocean temperatures during the past 5000 years reconstructed from the EPICA Dome C ice core, *Holocene*, *14*(2), 145–151.

Mayewski, P. A., et al. (2004), Holocene climate variability, *Quat. Res.*, *62*, 243–255.

Mendoza, B. (1997), Estimations of Maunder minimum solar irradiance and Ca II H and K fluxes using rotation rates and diameters, *Astrophys. J.*, *483*, 523–526.

Nielsen, S. H. H., N. Koç, and X. Crosta (2004), Holocene climate in the Atlantic sector of the Southern Ocean: Controlled by insolation or oceanic circulation, *Geology*, *32*(4), 317–320.

Osborn, T. J. (1997), Thermohaline oscillations in the LSG OGCM: Propagating anomalies and sensitivity to parameterizations, *J. Phys. Oceanogr.*, *27*, 2233–2255.

Pierce, D. W., T. P. Barnett, and U. Mikolajewicz (1995), Competing role of heat and freshwater flux in forcing thermohaline oscillations, *J. Phys. Oceanogr.*, *25*, 2046–2064.

Poore, R. Z., H. J. Dowsett, S. Verardo, and T. M. Quinn (2003), Millennial- to century-scale variability in Gulf of Mexico Holocene climate records, *Paleoceanography*, *18*(2), 1048, doi:10.1029/2002PA000868.

Presti, M., L. D. Santis, M. Busetti, and P. T. Harris (2003), Late Pleistocene and Holocene sedimentation on the George V Continental Shelf, East Antarctica, *Deep Sea Res., Part II*, *50*(8–9), 1441–1461.

Rathburn, A. E., J. J. Pichon, M. A. Ayress, and P. DeDeckker (1997), Microfossil and stable-isotope evidence for changes in Late Holocene paleoproductivity and paleoceanographic conditions in the Prydz Bay region of Antarctica, *Palaeogeogr. Palaeoclimatol. Palaeoecol.*, *131*, 485–510.

Renssen, H., H. Goosse, T. Fichefet, V. Masson-Delmotte, and N. Koç (2005), Holocene climate evolution in the high-latitude Southern Hemisphere simulated by a coupled atmosphere-sea-ice-ocean-vegetation model, *Holocene*, *15*(7), 951–964.

Renssen, H., H. Goosse, and R. Muscheler (2006), Coupled climate model simulation of Holocene cooling events: Oceanic feedback amplifies solar forcing, *Clim. Past*, *2*, 79–90.

Rind, D. (2002), The sun's role in climate variations, *Science*, *296*, 673–677.

Sarnthein, M., S. Kreveld, H. Erlenkeuser, P. M. Grootes, M. Kucera, U. Pflaumann, and M. Schulz (2003), Centennial-to-millennial scale periodicities of Holocene climate and sediment injections off the western Barents shelf, 75°N, *Boreas*, *32*, 447–461.

Schrader, H. J., and R. Gersonde (1978), Diatoms and silicoflagellates, in *Micropaleontological Counting Methods and Techniques—An Exercise on an Eight Meters Section of the Lower Pliocene of Capo Rossello, Silicy*, *Utrecht Micropaleontol. Bull.*, vol. 17, edited by E. Zaccharias et al., pp. 129–176, U. M. B., Odijk, Netherlands.

Schulz, M., and M. Muldesee (2002), REDFIT: Estimating red-noise spectra directly from unevenly spaced paleoclimatic time series, *Comput. Geosci.*, *28*, 421–426.

Sharma, M. (2002), Variations in solar magnetic activity during the last 200,000 years: Is there a Sun-climate connection?, *Earth Planet. Sci. Lett.*, *199*, 459–472.

Shindell, D., D. Rind, N. Balachandran, J. Lean, and P. Lonergan (1999), Solar cycle variability, ozone, and climate, *Nature*, *284*, 305–308.

Silvestri, G. E., and C. S. Vera (2003), Antarctic oscillation signal on precipitation anomalies over southeastern South America, *Geophys. Res. Lett.*, *30*(21), 2115, doi:10.1029/2003GL018277.

Simmonds, I. (1996), Climatic role of Southern Hemisphere extratropical cyclones and their relationships with sea-ice, *Pap. Proc. R. Soc. Tasmania*, *130*(2), 95–100.

Stuiver, M., G. H. Denton, T. J. Hugues, and J. L. Fastook (1981), History of the marine ice sheet in West Antarctica during the last deglaciation: A working hypothesis, in *The Last Great Ice Sheet*, edited by G. H. Denton, and T. J. Hugues, pp. 319–346, John Wiley, New York.

Stuiver, M., P. J. Reimer, E. Bard, J. W. Beck, G. S. Burr, K. A. Hughen, B. Kromer, G. McCormac, J. van de Plicht, and M. Spurk (1998a), INTCAL98 radiocarbon age calibration, 24.000–0 cal BP, *Radiocarbon*, *40*(3), 1041–1083.

Stuiver, M., P. J. Reimer, and T. F. Braziunas (1998b), High-precision radiocarbon age calibration for terrestrial and marine samples, *Radiocarbon*, *40*(3), 1127–1151.

Svensmark, H. (2000), Cosmic rays and Earth's climate, *Space Sci. Rev.*, *93*, 175–195.

Svensmark, H., and E. Friis-Christensen (1997), Variation of cosmic ray flux and global cloud coverage: A missing link in solar-climate relationships, *J. Atmos. Sol. Terr. Phys.*, *59*, 1225–1232.

Taylor, F., and A. McMinn (2001), Evidence from diatoms for Holocene climate fluctuation along the East Antarctic Margin, *Holocene*, *11*(4), 455–466.

Taylor, F., J. Whitehead, and E. Domack (2001), Holocene paleoclimate change in the Antarctic Peninsula: Evidence from the diatom, sedimentary and geochemical record, *Mar. Micropaleontol.*, *41*, 25–43.

Torrence, C., and G. P. Compo (1998), A practical guide to wavelet analysis, *Bull. Am. Meteorol. Soc.*, *79*(1), 61–78.

Turney, C., M. Baillie, S. Clemens, D. Brown, J. Palmer, J. Pilcher, P. Reimer, and H. H. Leuschner (2005), Testing solar forcing of pervasive Holocene climate cycles, *J. Quat. Sci.*, *20*(6), 511–518.

Warner, N. R., and E. W. Domack (2002), Millennial- to decadal-scale paleoenvironmental change during the Holocene in the Palmer Deep, Antarctica, as recorded by particle size analysis, *Paleoceanography*, *17*(3), 8004, doi:10.1029/2000PA000602.

White, W. B., and R. G. Peterson (1996), An Antarctic circumpolar wave in surface pressure, wind, temperature and sea-ice extent, *Nature*, *380*, 699–702.

Wright, S. W., and R. L. van den Enden (2000), Phytoplankton community structure and stocks in the East Antarctic Marginal ice zone (BROKE survey, January–March 1996) determined by CHEMTAX analysis of HPLC pigment signatures, *Deep Sea Res., Part II*, *47*, 2363–2400.

Yuan, X. (2004), ENSO-related impacts on Antarctic sea ice: A synthesis of phenomena and mechanisms, *Antarct. Sci.*, *16*(4), 415–425.

Zielinski, U., and R. Gersonde (1997), Diatom distribution in Southern Ocean surface sediments (Atlantic Sector): Implications for paleoenvironmental reconstructions, *Palaeogeogr. Palaeoclimatol. Palaeoecol.*, *129*, 213–250.